NANO TWIST AND SHOUT: CHIRAL NANOANTENNAS MAKING WATER SPLITTING COOL

[1]Jana ROSENKRAZOVA, [1]Elena MILIUTINA, [1]Vasilii BURTSEV, [1]Vaclav SVORCIK, [1]Oleksiy LYUTAKOV

[1]University of Chemistry and Technology, Prague, Czech Republic, EU, rosenkrj@vscht.cz

https://doi.org/10.37904/nanocon.2025.4989

Abstract

In the last several years, spin polarization of electrons has been reported as a promising method of improving oxygen evolution reaction (OER). Here, we report the development of a system of hybrid multilayer materials with a chiral property for light-assisted water splitting. The chiral electrodes were prepared via a thin patterned metal film, with a dielectric layer. A layer of redox-active was deposited on the top of prepared structure. The resulting samples were characterized at each step of their preparation using SEM-EDX methods. It is hypothesized that electron spin polarization suppresses the formation of hydrogen peroxide and promote the formation of triplet state of O_2 during OER. This assumption was confirmed via electrochemical measurements, particularly using linear sweep voltammetry and chronoamperometry. During the experiments, we found a correlation between the OER efficiency and the electrode chirality.

Keywords: Chiral electrode, hybrid structure, OER, water splitting

1. INTRODUCTION

In recent years, plasmonic nanoantennas have emerged as a promising technology in the field of plasmon-assisted water splitting [1 ,2], possibly paving the way for the future of efficient green hydrogen production [2–4]. Capable of efficiently converting free-propagating optical radiation to localized energy [5] beyond the diffraction limit [6–8] and vice versa [5,6], plasmonic nanoantennas operate on the principle of absorbing the incident electromagnetic radiation at a resonant frequency, which causes movement of free electrons in the plasmonic material and thus generating an alternating electric current [5].

While geometry [5–7], used materials [5,7] and the dielectric environment [6,7] of the nanoantenna significantly affect their properties [1,5–7], the addition of a chiral element to the structure allows for more subtle optical effects, with light propagation and absorption being different for left and right circularly polarized light [9].Chirality can be introduced through meticulous design [9,10] or the addition of chiral substances to the otherwise non-chiral structures [10,11]. In both cases, chirality of the structure imposes a chiral character on the oscillation of free electrons on the electrode surface and bulk [12]. Another important property of chiral structures is the chiral-induced spin selectivity (CISS) effect, which causes spin the polarisation of an electron [13]. In other words, the CISS effect implies the chiral substance preferentially transmits electrons with one spin direction [14].

For water splitting in particular, the sluggish kinetics of oxygen evolution reaction (OER) [13–16] prevent it from being used on a large scale for green hydrogen production [13,14]. During the water splitting process, the interaction of OH^* radicals intermediates determines the formation of either an oxygen molecule or hydrogen peroxide [14]. By allowing the transfer of parallel spin-oriented electrons only, the formation of H_2O_2 is significatnly reduced, thus enhancing the creation of O_2 [14,16]. The differences between chiral and achiral structures for OER, the utilization of spin-control for catalysis and reaction products are represented in **Figure 1** [15]. In this work, we propose a hybrid multilayer structure, which acts as a chiral lock, enhancing the efficiency of a previously proposed design [1].

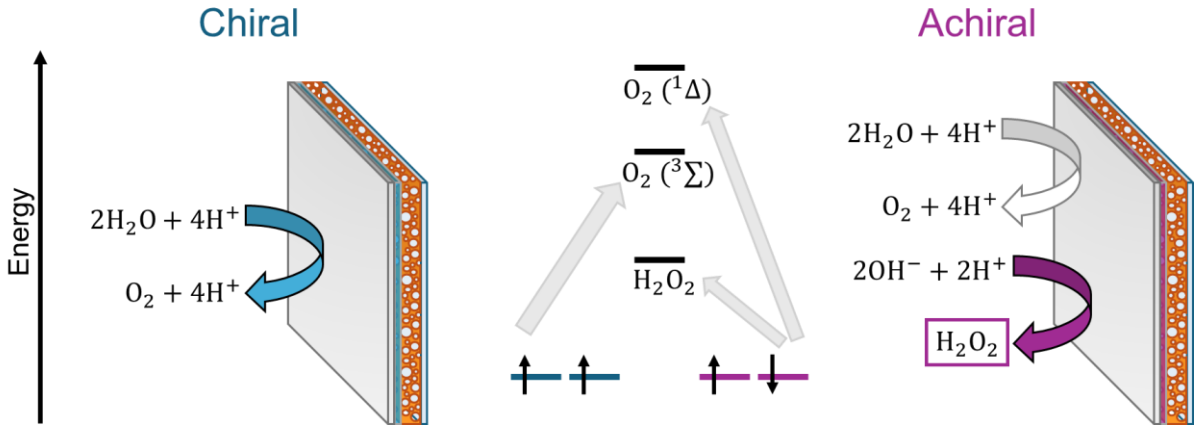

Figure 1 Scheme of chiral and achiral nanoantennas and their utilization for OER, electron spins participating in the reaction, energetic states of potential reaction products and preferential reaction paths

2. EXPERIMENTAL SECTION

2.1 Materials

All chemical substances used for the preparation of the samples are provided in **Table 1**. Platinum target with 4N purity from SAFINA a.s. was used for thin-film preparation. FTO coated glass (TEC 7 FTO) was purchased from MSE Supplies™. Other chemicals used were demineralized water (demi-H_2O) and potassium hydroxide (KOH, 1 mol L^{-1}) from Sigma-Aldrich.

Table 1 Chemical substances used for sample preparation

Substance	Full name	Purity (%)	Manufacturer
PS-*b*-PEO	Poly(styrene-*b*-ethylene oxide)	100	Polymer Source, Inc.
$H_7AuCl_4O_3$	Hydrogen tetrachloroaurate (III) trihydrate	(Au) 49.5	Abcr GmbH
THF	Tetrahydrofuran	99.95	Lach-Ner, s.r.o.
EtOH	Ethanol for analysis	100	Merck
PS	Polystyrene	100	SigmaAldrich
Toluene	Toluene	≥99.9	Lach-Ner, s.r.o.
$C_4H_6NiO_4 \cdot 4H_2O$	Nickel(II) acetate tetrahydrate	≥98	SigmaAldrich
-	Hydrogen peroxide test	-	SigmaAldrich

2.2 Sample preparation

First, a micelle solution was prepared for the preparation of mesoporous gold (porAu). 10 mg of PS-*b*-PEO was weighed and dissolved in 3 ml of THF and left in a water bath (40 °C, 30 min, 275 rpm). Then, 1.5 ml of EtOH was slowly added, followed by 1 ml of 40 mM $HAuCl_4$ and 2.5 ml of demi-H_2O, and the solution was kept at 40 °C for 1 hour. For the preparation of the patterned gold layer, chronoamperometry ($E_{dc} = -0.5$ V, $t_{\mathrm{run}} = 1200$ s) was used in a 5 ml beaker in a three-electrode system with an FTO glass as the working electrode, Ag/AgCl (3 M KCl) as the reference electrode (BVT Technologies, CZ), and a platinum wire as the counter electrode (BASi, USA). PalmSens 4 potentiostat (Palm Instruments, Netherlands) with PSTrace 5.8 software was used for all electrochemical measurements. After chronoamperometric deposition, the FTO

glasses with the gold layer were carefully washed alternately in THF and demi-H_2O seven times using a pipette. This preparation was adapted from Li et al. [17].

Subsequently, a dielectric chiral spacer was deposited. Finally, a thin layer of Pt (Quorum Q300T, 20 mA, 110 s, Ar atmosphere) was sputtered. Scheme of the samples' preparation is shown in **Figure 2**. Finally, NiO_x was grown by electrodeposition at -1 V vs. Ag/AgCl (3M KCl) for 200 s in an aqueous electrolyte containing 20 mM $C_4H_6NiO_4 \cdot 4H_2O$.

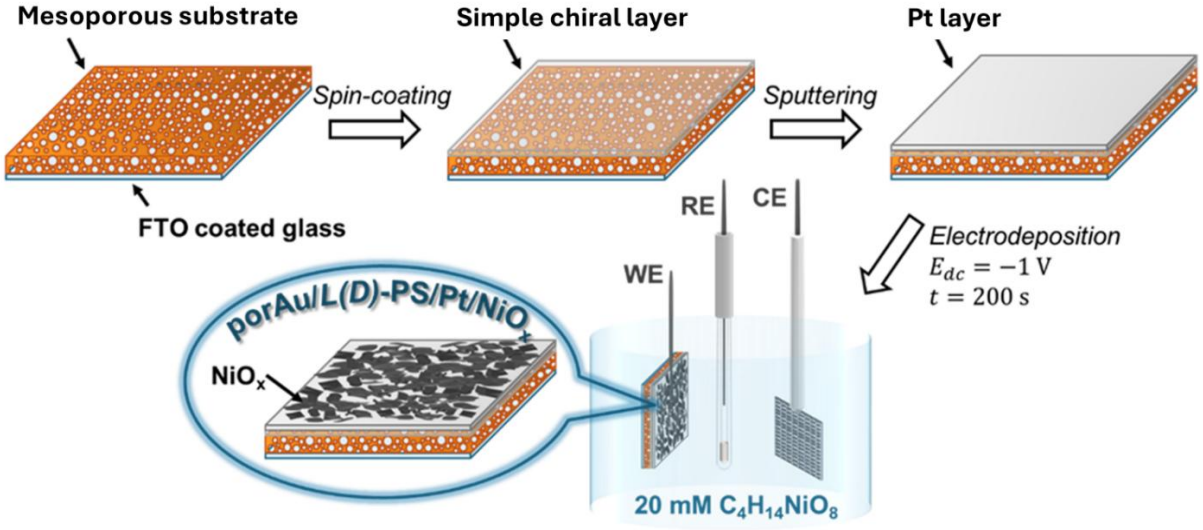

Figure 2 Nanoantenna samples' preparation

2.3 Measurement techniques

To study the surface of the samples at multiple stages of preparation, scanning electron microscopy (SEM) and energy-dispersive X-ray spectroscopy (EDX) (LYRA3 GMU, Tescan, CR) were collected at the operating voltage of 10 kV and a beam current of 600 pA. To better understand the absorption of light of the samples, UV-Vis spectra was obtained using UV/VIS spectrometer HR2000 (Ocean Optics) with AvaLight-DHS light source (Avantes).

2.4 Electrochemical measurements

LSV and chronoamperometry were used for electrochemical analysis in a classic three-electrode system in a 5 ml beaker. The samples were attached as the working electrode, Ag/AgCl (sat. with 3 M KCl) electrode (BVT Technologies, CZ) as the reference electrode and a Platinum Wire electrode (BASi, USA) as the counter electrode, with 0.1 M KOH as the electrolyte.

2.5 H_2O_2 determination

Tests for the presence of H_2O_2 were performed by chronoamperometry in 0.1 M KOH saturated with CO_2 to reduce H_2O_2 decomposition. Each chronoamperometry measurement lasted 20 min at 2 V against Ag/AgCl to sufficiently produce H_2O_2. The electrolytes were then transferred to cleaned polypropylene centrifuge tubes and the procedure indicated in the test instructions was carried out.

3. RESULTS AND DISCUSSION

To better organise the results, the following labels are used for the sample names: porAu/PS/Pt for achiral systems and porAu/L- or D-PS/Pt or for chiral systems. Systems without the dielectric layer are labelled porAu/Pt.

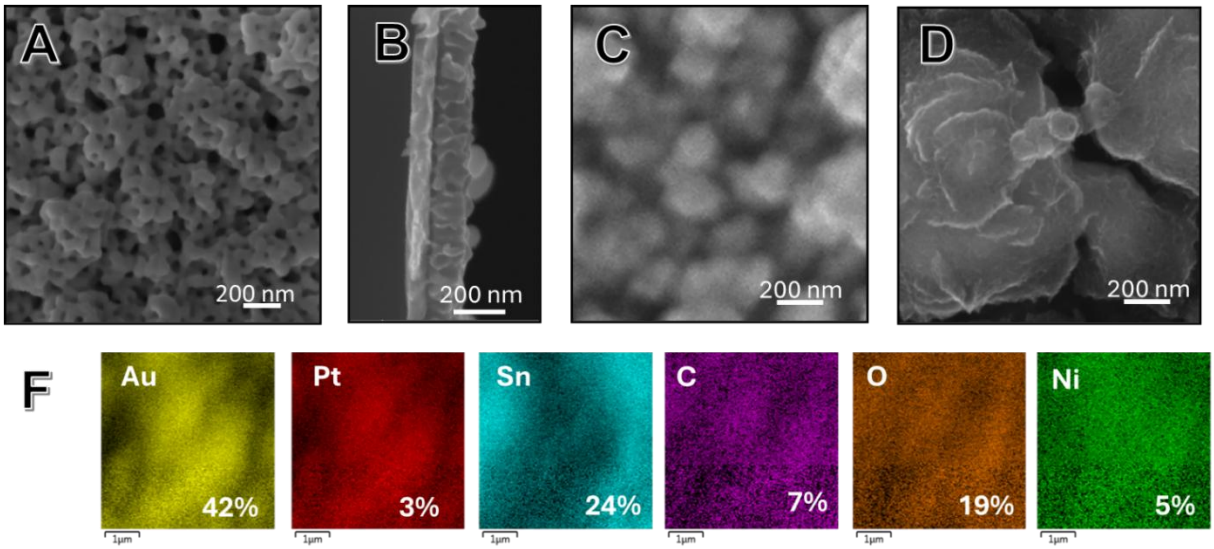

Figure 3 SEM images of nanoantennas at each preparation step: porAu (A), porAu cross-section (B), porAu/L-PS/Pt (C) and porAu/L-PS/Pt/NiO_x (D)

Figure 3 shows the SEM images of all samples containing a chiral or non-chiral dielectric layer with a layer of Pt and NiO_x on top. As expected, sample porAu has pores in the order of 20 - 50 nm. From a cross-section of the sample, the thickness of the mesoporous gold layer was determined as ~180 nm (**Figure 3B**). As expected, after the dielectric and Pt layers deposition, the surface is smoother, and no pores are observed. Surface morphology after NiO_x deposition is presented in **Figure 3D**. In addition, **Figure 3E** shows EDX analysis data, which confirms the presence of Au, Pt and Ni elements on the samples' surface.

Figure 4A shows LSV measurements of chiral and achiral nanoantennas. At first, the LSV was left to run in the dark. After, the light was turned on, as indicated in the figure. The results show that the activity of chiral hybrid structures is much higher than their non-chiral counterparts. This is in agreement with spin-control reaction theory, as explained above [14–16].

Figure 4B shows UV-Vis spectra of the solution analysed for the presence of H_2O_2, as described above. The presence of hydrogen peroxide was clearly detected for both analysed samples with the light off. However, the addition of a chiral substance to the nanoantenna caused the detected amount to decrease significantly while the reaction was left to run with the light on compared to the achiral. This behaviour is, once again, in agreement with spin-control reaction theory, as explained above [14–16].

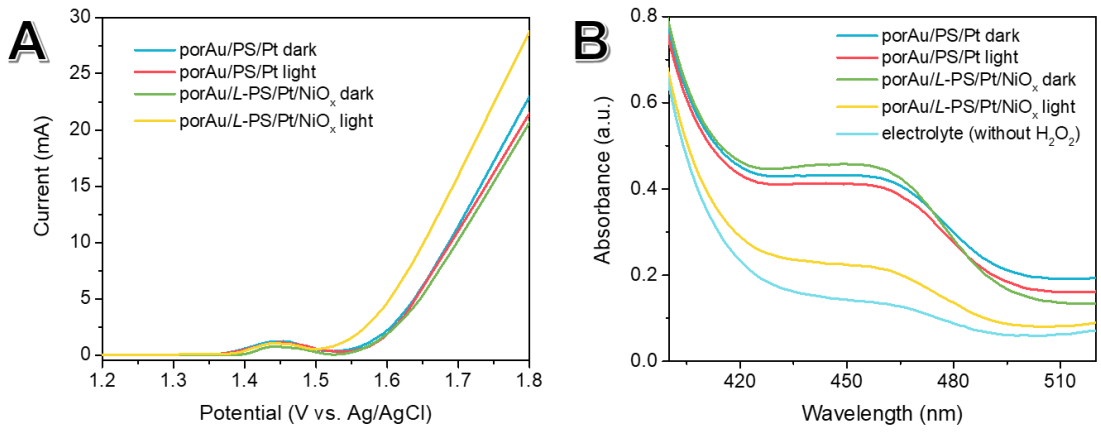

Figure 4 OER activity of chiral and non-chiral nanoantennas in 0.1 M KOH (A) and UV-Vis results of H_2O_2 formation from chronoamperometry at 2 V vs. Ag/AgCl obtained on chiral and achiral structures under and without light (B). The absorption spectra were normalized by the total charge transferred during the reaction.

4. CONCLUSION

In this work, a new way to improve OER was found – using chiral multilayer materials. The incorporation of chiral substances into an already sufficiently efficient system, the rate of the OER exhibited a sharp increase due to the CISS effect, allowing only electrons of a certain spin to participate in the reaction and thus reducing the H_2O_2 production. Therefore, chiral nanoantennas represent a largely unexplored system with significant potential for improving OER.

ACKNOWLEDGEMENTS

This work was supported by the GACR under project 23-08509S.

REFERENCES

[1] ROSENKRANZOVA, J.; BURTSEV, V.; MILIUTINA, E.; SVORCIK, V.; LYUTAKOV, O. Creation of Plasmon-Based Nanoantenna for Hydrogen Production. In: *NANOCON 2023*. Ostrava: Tanger, 2023, pp. 94–99. Available from: https://doi.org/10.37904/nanocon.2023.4754.

[2] GHOBADI, T. G. U.; GHOBADI, A.; SOYDAN, M. C.; VISHLAGHI, M. B.; KAYA, S.; KARADAS, F.; OZBAY, E. Strong Light–Matter Interactions in Au Plasmonic Nanoantennas Coupled with Prussian Blue Catalyst on BiVO4 for Photoelectrochemical Water Splitting. *ChemSusChem.* 2020, vol. 13, no. 10, pp. 2577–2588. Available from: https://doi.org/10.1002/cssc.202000294.

[3] HASSAN, N. S.; JALIL, A. A.; RAJENDRAN, S.; KHUSNUN, N. F.; BAHARI, M. B.; JOHARI, A.; KAMARUDDIN, M. J.; ISMAIL, M. Recent Review and Evaluation of Green Hydrogen Production via Water Electrolysis for a Sustainable and Clean Energy Society. *International Journal of Hydrogen Energy.* 2024, vol. 52, pp. 420–441. Available from: https://doi.org/10.1016/j.ijhydene.2023.09.068.

[4] Di GARBO, C.; LIVRERI, P.; VITALE, G. Solar Nanoantennas Energy Based Characterization. *Renewable Energy and Power Quality Journal.* 2016, vol. 1, pp. 862–867. Available from: https://doi.org/10.24084/repqj14.490.

[5] LI, N.; LAI, Y.; LAM, S. H.; BAI, H.; SHAO, L.; WANG, J. Directional Control of Light with Nanoantennas. *Advanced Optical Materials.* 2021, vol. 9, no. 1, 2001081. Available from: https://doi.org/10.1002/adom.202001081.

[6] KRASNOK, A. E.; MAKSYMOV, I. S.; DENISYUK, A. I.; BELOV, P. A.; MIROSHNICHENKO, A. E.; SIMOVSKI, C. R.; KIVSHAR, Y. S. Optical Nanoantennas. *Phys.-Usp.* 2013, vol. 56, no. 6, 539. Available from: https://doi.org/10.3367/UFNe.0183.201306a.0561.

[7] ZABELINA, A.; MILIUTINA, E.; ZABELIN, D.; BURTSEV, V.; BURAVETS, V.; ELASHNIKOV, R.; NEUBERTOVA, V.; ŠŤASTNÝ, M.; POPELKOVÁ, D.; LANCOK, J.; CHERTOPALOV, S.; PAIDAR, M.; TRELIN, A.; MICHALCOVÁ, A.; ŠVORČÍK, V.; LYUTAKOV, O. Plasmon Coupling inside 2D-like TiB2 Flakes for Water Splitting Half Reactions Enhancement in Acidic and Alkaline Conditions. *Chemical Engineering Journal.* 2023, vol. 454, 140441. Available from: https://doi.org/10.1016/j.cej.2022.140441.

[8] KRAVETS, V. G.; BARNES, W. L.; KABASHIN, A. V.; GRIGORENKO, A. N. Plasmonic Surface Lattice Resonances: A Review of Properties and Applications. *Chemical Reviews.* 2018, vol. 118, no. 12, pp. 5912–5951. Available from: https://doi.org/10.1021/acs.chemrev.8b00243.

[9] KIM, M.; BAZAID, M. O.; LEE, H. J.; JANG, S. S.; JANG, Y. J.; KIM, D. H. Chiral Inorganic Nanostructures from Achiral Platforms: A Universal Synthesis Route via Supramolecular Self-Assembly. *Chem. Mater.* 2023, vol. 35, no. 8, pp. 3073–3082. Available from: https://doi.org/10.1021/acs.chemmater.2c02833.

[10] KALACHYOVA, Y.; GUSELNIKOVA, O.; ELASHNIKOV, R.; PANOV, I.; ŽÁDNÝ, J.; CÍRKVA, V.; STORCH, J.; SYKORA, J.; ZARUBA, K.; ŠVORČÍK, V.; LYUTAKOV, O. Helicene-SPP-Based Chiral Plasmonic Hybrid Structure: Toward Direct Enantiomers SERS Discrimination. *ACS Appl. Mater. Interfaces.* 2019, vol. 11, no. 1, pp. 1555–1562. Available from: https://doi.org/10.1021/acsami.8b15520.

[11] GOERLITZER, E. S. A.; PURI, A. S.; MOSES, J. J.; POULIKAKOS, L. V.; VOGEL, N. The Beginner's Guide to Chiral Plasmonics: Mostly Harmless Theory and the Design of Large-Area Substrates. *Advanced Optical Materials.* 2021, vol. 9, no. 16, 2100378. Available from: https://doi.org/10.1002/adom.202100378.

[12] LIANG, Y.; BANJAC, K.; MARTIN, K.; ZIGON, N.; LEE, S.; VANTHUYNE, N.; GARCÉS-PINEDA, F. A.; GALÁN-MASCARÓS, J. R.; HU, X.; AVARVARI, N.; LINGENFELDER, M. Enhancement of Electrocatalytic Oxygen Evolution by Chiral Molecular Functionalization of Hybrid 2D Electrodes. *Nat Commun.* 2022, vol. 13, no. 1, 3356. Available from: https://doi.org/10.1038/s41467-022-31096-8.

[13] MINGOES, C. J.; SCHROEDER, B. C.; JORGE SOBRIDO, A. B. Electron Spin Selective Iridium Electrocatalysts for the Oxygen Evolution Reaction. *ACS Mater. Au.* 2024, vol. 4, no. 2, pp. 204–213. Available from: https://doi.org/10.1021/acsmaterialsau.3c00084.

[14] GHOSH, K. B.; ZHANG, W.; TASSINARI, F.; MASTAI, Y.; LIDOR-SHALEV, O.; NAAMAN, R.; MÖLLERS, P.; NÜRENBERG, D.; ZACHARIAS, H.; WEI, J.; WIERZBINSKI, E.; WALDECK, D. H. Controlling Chemical Selectivity in Electrocatalysis with Chiral CuO-Coated Electrodes. *J. Phys. Chem. C.* 2019, vol. 123, no. 5, pp. 3024–3031. Available from: https://doi.org/10.1021/acs.jpcc.8b12027.

[15] NAAMAN, R.; PALTIEL, Y.; WALDECK, D. H. Chiral Induced Spin Selectivity Gives a New Twist on Spin-Control in Chemistry. *Acc. Chem. Res.* 2020, vol. 53, no. 11, pp. 2659–2667. Available from: https://doi.org/10.1021/acs.accounts.0c00485.

[16] LI, C.; JIANG, B.; CHEN, H.; IMURA, M.; SANG, L.; MALGRAS, V.; BANDO, Y.; AHAMAD, T.; ALSHEHRI, S. M.; TOMINAKA, S.; YAMAUCHI, Y. Superior Electrocatalytic Activity of Mesoporous Au Film Templated from Diblock Copolymer Micelles. *Nano Res.* 2016, vol. 9, no. 6, pp. 1752–1762. Available from: https://doi.org/10.1007/s12274-016-1068-z.